The effect of ancillary ligands on hydrocarbon C-H bond functionalization by uranyl photocatalysts

Ryte Rutkauskaite,[a,b] Xiaobin Zhang,[c] Adam W. Woodward,[d] Yanlin Liu,[a] Gabriel Herrera,[a] Jamie Purkis,[e] Sean D. Woodall,[f] Mark Sarsfield,[f] H. Georg Schreckenbach,[c] Louise S. Natrajan,[d]* Polly L. Arnold [a,b]*

[a]Department of Chemistry, University of California, Berkeley, California 94720 (USA)
[b] Lawrence Berkeley National Laboratory, California 94720 (USA)
[c] Department of Chemistry, University of Manitoba, Winnipeg, Manitoba, Canada R3T 2N2
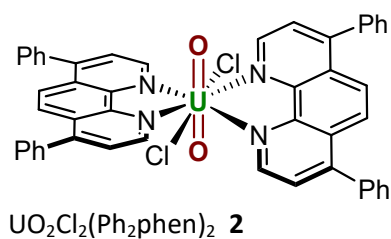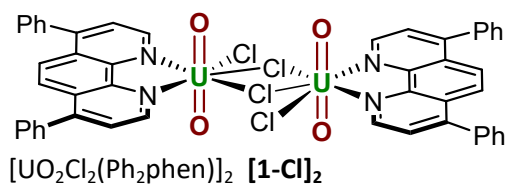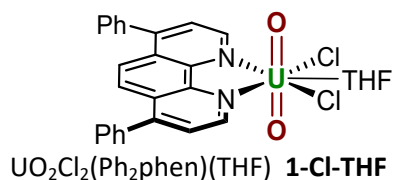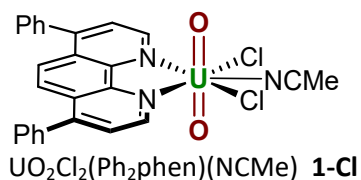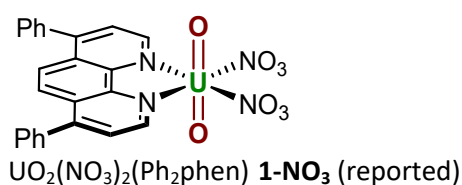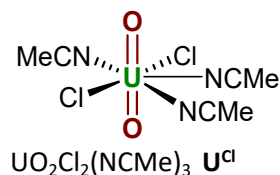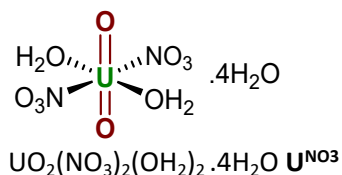[d] Department of Chemistry, University of Manchester, Manchester M13 9PL (UK)
[e] Atkins (part of SNC-Lavalin Group), The Hub 500 Park Avenue, Aztec West, Bristol BS32 4RZ, United Kingdom
[f] UK National Nuclear Laboratory, Central Laboratory, Sellafield, Seascale, Cumbria, CA20 1PG, United Kingdom

Contents

1. Compound numbering scheme:

UO$_2$(NO$_3$)$_2$(OH$_2$)$_2$·4H$_2$O **U^{NO3}**

UO$_2$Cl$_2$(NCMe)$_3$ **U^{Cl}**

UO$_2$(NO$_3$)$_2$(Ph$_2$phen) **1-NO$_3$** (reported)

UO$_2$Cl$_2$(Ph$_2$phen)(NCMe) **1-Cl**

UO$_2$Cl$_2$(Ph$_2$phen)(THF) **1-Cl-THF**

[UO$_2$Cl$_2$(Ph$_2$phen)]$_2$ **[1-Cl]$_2$**

UO$_2$Cl$_2$(Ph$_2$phen)$_2$ **2**

2. General experimental details, materials and methods

Solvents and reagents. Bathophenanthroline (ph$_2$phen) was purchased from Sigma Aldrich and purified before use by dissolving it in methanol, running the solution through a silica plug, and removing volatiles in *vacuo*. The solid was then recrystallized from hot toluene. Other chemicals and solvents were purchased from Sigma Aldrich or Fisher Scientific. Deuterated solvents were purchased from Cambridge Isotope Laboratories. Solids used for anaerobic reactions (uranyl complexes, *N*-fluorobenzenesulfonimide) were dried under vacuum on a high-vacuum Schlenk-line overnight before use. Cyclooctane was freeze-pump-thaw degassed three times and stored over 3 Å molecular sieves under an N$_2$ atmosphere for one week before use. Acetonitrile was dried using an MBRAUN SPS 800 Manual solvent purification system and stored over activated 3 Å molecular sieves. CD$_3$CN was dried

over calcium hydride before being freeze-pump-thaw degassed three times and purified by trap-to-trap distillation. **1-NO$_3$** was synthesized according to a literature procedure.[1]

Characterization. NMR spectra were recorded on Bruker Avance 400, 500 and 600 MHz spectrometers and referenced to solvent residual signals (^{1}H, ^{13}C). Acetonitrile was used as solvent for no-deuterium NMR experiments and was referenced to the solvent peak (1.94 ppm). Chemical shifts are quoted in ppm and coupling constants in Hz. NMR spectra were taken at 25°C. UV/vis spectra were recorded with a Varian Cary 50 spectrophotometer, sing quartz cells with a 10 mm pathlength equipped with a J-Young valve with samples prepared under a dinitrogen atmosphere. ATR-IR spectra were recorded using a Thermo Scientific Nicolet iS10 FTIR or a Shimadzu IRSpirit FTIR spectrometer. Absorption bands are reported in wavenumbers (cm^{-1}) with a note on intensity: s – strong; m – medium; w – weak. Elemental analyses were carried out by Dr. Elena Kreimer at the microanalytic facility in the College of Chemistry at the University of California, Berkeley with a Perkin Elmer CHNS 2400 Series II analyzer. GC analyses and calibration curves were obtained on an Agilent 6890 GC equipped with an HP-5 column (25 m x 0.20 mm ID x 0.33 m film) and an FID detector.

Absorption/emission spectroscopy. UV-vis electronic absorption spectra were recorded on a Mettler Toledo UV5Bio spectrophotometer. Steady state emission and excitation spectra and lifetime data were recorded on an Edinburgh Instruments FP920 phosphorescence spectrometer or an Edinburgh Instruments FLS-1000 photoluminescence spectrometer. The FP920 spectrometer is equipped with a 450 W steady state xenon lamp, a 5 W microsecond pulsed xenon flash lamp, (with single 300 mm focal length excitation and emission monochromators in Czerny Turner configuration), interchangeable EPL pulsed diode lasers, and a red sensitive photomultiplier in Peltier (air cooled) 53 housing (Hamamatsu R928P). The FLS-1000 spectrometer is equipped with a 450 W steady state xenon lamp, a 100 W microsecond pulsed xenon flash lamp, (with double 325 mm focal length excitation and emission monochromators in Czerny Turner configuration), interchangeable EPL pulsed diode lasers, and a red sensitive photomultiplier in Peltier (air cooled) 53 housing (Hamamatsu R928P). Plotting, fitting and analysis of data was carried out using Origin 2019b. All data were fitted with exponential decay models and the goodness of fit evaluated by the residual, χ^2 and R^2 analysis.

3. Syntheses

UO$_2$Cl$_2$(MeCN). Uranyl chloride hydrate (UO$_2$Cl$_2$·3H$_2$O) was stirred in dry MeCN for 1 hr. The solvent was then removed *in vacuo* and the resulting yellow solid was further dried *in vacuo* for 5 hrs. The solid is sparingly soluble in MeCN and pyridine, and is not soluble in chloroform, DCM, chlorobenzene, and *ortho*-difluorobenzene. Crystals of the complex were grown from a concentrated MeCN solution at –30°C in an N$_2$ atmosphere glovebox, but desolvated immediately when put on a microscope slide. The NMR spectrum of the dried solid in DMSO with a methyl acetate internal standard shows 1 equivalent of MeCN coordinated to uranyl chloride.

^{1}H NMR (400 MHz, DMSO-d$_6$): δ 2.04 (CH$_3$CN). **UV/vis** (MeCN), λ_{max}/nm: 244, 433. The ε values could not be calculated due to low solubility of the complex in acetonitrile. **FTIR** (cm^{-1}): 2308 (w), 2280 (w), 1357 (w), 953 (s). **Elemental analysis**: expected C, 6.29%, H, 0.79%, N, 3.67%; found C, 6.70%, H, 0.86%, N, 3.85%.

UO$_2$Cl$_2$(Ph$_2$phen)(MeCN) (1-Cl). The slow addition of an acetonitrile suspension of 1 equivalent of ph$_2$phen to a stirred acetonitrile solution of a uranyl chloride hydrate (UO$_2$Cl$_2$·3H$_2$O) in acetonitrile results in a color change from yellow to light orange. A small amount of fluorescent yellow precipitate (the *bis*-ph$_2$phen complex **2**) forms as well. The subsequent removal of solvent *in vacuo* yields an orange solid that is soluble in acetonitrile and acetone. Attempts to crystallize the complex from MeCN were unsuccessful, however, the THF solvate **UO$_2$Cl$_2$(Ph$_2$phen)(THF) (1-Cl-THF)** was crystallized by vapor diffusion of hexanes to a THF solution of **1-Cl-MeCN**. **^{1}H NMR** (400 MHz, CD$_3$CN): δ 11.26 (s, 2H, N=CH$_{phen}$), 8.18 (s, 4H, CH$_{phen}$), 7.65 (d, J = 5.5 Hz, 10H, CH$_{ph}$). **UV/vis** (MeCN), λ_{max}/nm (ε/M^{-1} cm^{-1}): 421-484 (56 at 452 nm). **High resolution mass spectrometry** Calculated for [C$_{24}$H$_{16}$Cl$_2$N$_2$O$_2$U]+ (M)+

m/z 672.1097, found 672.1070 (difference -4.0172017 ppm). **E_{red} (MeCN, TBA-BPh$_4$) = -1.163 eV vs Fc$^+$/Fc**

[UO$_2$Cl$_2$(Ph$_2$phen]$_2$ ([1-Cl]$_2$. Crystals of the dimer **[1-Cl]$_2$** were grown by vapor diffusion of hexanes to a chlorobenzene solution of crude **1-Cl-MeCN**. The NMR spectrum of **[1-Cl]$_2$** in CD$_3$CN is identical to that of **1-Cl-MeCN**. **FTIR** (cm^{-1}): 943 (s). **UV/vis** (DCM), λ_{max}/nm: 422-486.

[UO$_2$Cl$_2$(Ph$_2$phen)(THF)] Crystals of [UO$_2$Cl$_2$(ph$_2$phen)(THF)] were grown by vapour diffusion of hexanes to a THF solution of [UO$_2$Cl$_2$(ph$_2$phen)(MeCN)].

UO$_2$Cl$_2$(Ph$_2$phen)$_2$ (2). The addition of an acetonitrile suspension of UO$_2$Cl$_2$·3H$_2$O (440.2 mg; 1.128 mmol) to a stirred suspension of 2 equivalents of ph$_2$phen (750.0 mg; 2.256 mmol), also in acetonitrile, immediately resulted in the precipitation of a fluorescent yellow powder. The solid was then washed sequentially with acetonitrile and diethyl ether, and dried *in vacuo* to yield [UO$_2$Cl$_2$(Ph$_2$phen)$_2$] **2** (1.0122 g; 89% yield). The solid is insoluble in acetonitrile or acetone but is sparingly soluble in chloroform and DCM. Single crystals suitable for SC-XRD were grown by layering a DCM solution of the complex with hexanes. In the IR spectrum of the complex, v_{asym}(U=O) appears at 900 cm^{-1}, which shows that the U=O bond is significantly weakened compared to the complex with one ph$_2$phen ligand discussed above (922 cm^{-1}). The (U=O) asymmetric stretch in a previously reported phenanthroline complex [UO$_2$Cl$_2$(phen)$_2$] is very similar (898 cm^{-1}).[3] **^{1}H NMR** (400 MHz, CD$_3$Cl): δ 10.14 (d, *J* = 5.2 Hz, 2H, N=CH$_{phen}$), 8.21 (s, 2H, CH$_{phen}$), 7.90 (d, *J* = 5.2 Hz, 2H, CH$_{phen}$) and 7.61 (m, 10H, CH$_{ph}$). **UV/vis** (MeCN), λ_{max}/nm (ε/M^{-1} cm^{-1}): 452 (218), 282 (43600). **FTIR** (cm^{-1}): 1560 (m), 1427 (m), 900 (s), 855 (m), 832 (m), 774 (m), 741 (m), 700 (s), 628 (m), 575 (m), 545 (m). **Elemental analysis**: expected C, 57.32%, H, 3.21%, N, 5.57%; found C, 56.09%, H, 3.07%, N, 5.34%.

Table S 1 UV-Vis electronic absorption spectral maxima for the complexes and ligand recorded in MeCN

Complex	λ_{max} (nm)
[UO$_2$(NO$_3$)$_2$(OH$_2$)$_2$]·4H$_2$O	423
[UO$_2$(NO$_3$)$_2$(Ph$_2$phen)]	427, 288
[UO$_2$Cl$_2$(ph$_2$phen)(MeCN)]	452,
[UO$_2$Cl$_2$(ph$_2$phen)$_2$]	453, 283
[UO$_2$Cl$_2$(MeCN)]	433
Ph$_2$phen	275

4. Crystallographic data

X-ray diffraction data for **[1-Cl-F]$_2$** were collected at beamline 12.2.1 of the Advanced Light Source (ALS) at Lawrence Berkeley National Lab, using a Bruker D8 diffractometer coupled to a Bruker PhotonII CPAD detector with Si(111)-monochromated synchrotron radiation (17 keV radiation). Absorption corrections were completed using APEX III software. All other single crystal X-ray diffraction data were collected using a Rigaku Xtalab Synergy-S diffractometer fitted with a HyPix-6000HE photon counting detector using MoKα (λ = 0.71073 Å) radiation. Absorption corrections were completed using CrysAlis PRO (Rigaku Oxford Diffraction) software. All structures were solved using SHELXT in Olex2 and refined using SHELXL in Olex2. Analytical numeric absorption corrections used a multifaceted crystal model based on expressions derived by Clark and Reid. Numerical absorption correction was based on a Gaussian integration over a multifaceted crystal model. All non-hydrogen atoms were refined with anisotropic displacement parameters and H-parameters were constrained to parent atoms and refined using a riding model.

Table S 2 Crystal data and structure refinement for **1-Cl-THF**, **[1-Cl]$_2$**, **2**, **[1-Cl-F]$_2$**

Complex	1-Cl-THF	[1-Cl]$_2$
Empirical formula	$C_{28}H_{24}Cl_2N_2O_3U$	$C_{60}H_{42}Cl_6N_4O_4U_2$
Formula weight	745.42	1571.73
Temperature/K	100.00(10)	99.98(12)
Crystal system	monoclinic	monoclinic
Space group	$P2_1/n$	C2/c
a/Å	9.06020(10)	14.4589(2)
b/Å	18.1719(2)	26.3459(4)
c/Å	15.7262(2)	14.4152(2)
α/°	90	90
β/°	97.1350(10)	89.3990(10)
γ/°	90	90
Volume/Å^3	2569.13(5)	5490.92(14)
Z	4	4
ρ_{calc}g/cm^3	1.927	1.901
μ/mm^{-1}	6.559	6.235
F(000)	1424.0	2992.0
Crystal size/mm^3	0.27 × 0.22 × 0.08	0.372 × 0.087 × 0.042
Radiation	Mo Kα (λ = 0.71073)	Mo Kα (λ = 0.71073)
2Θ range for data collection/°	3.44 to 54.968	4.188 to 55.754
Index ranges	-11 ≤ h ≤ 11, -23 ≤ k ≤ 23, -20 ≤ l ≤ 20	-18 ≤ h ≤ 19, -34 ≤ k ≤ 34, -18 ≤ l ≤ 18
Reflections collected	109761	115436
Independent reflections	5903 [R_{int} = 0.0525, R_{sigma} = 0.0178]	6560 [R_{int} = 0.0639, R_{sigma} = 0.0230]
Data/restraints/parameters	5903/0/325	6560/355/407
Goodness-of-fit on F^2	1.033	1.063
Final R indexes [I>=2σ (I)]	R_1 = 0.0167, wR_2 = 0.0363	R_1 = 0.0261, wR_2 = 0.0547
Final R indexes [all data]	R_1 = 0.0202, wR_2 = 0.0371	R_1 = 0.0426, wR_2 = 0.0623
Largest diff. peak/hole / e Å^{-3}	1.08/-0.60	2.21/-0.95

Table S 3 Crystal data and structure refinement for **1-Cl-THF**, **[1-Cl]$_2$**, **2**, **[1-Cl-F]$_2$**

Complex	2	[1-Cl-F]$_2$
Empirical formula	$C_{48}H_{32}Cl_2N_4O_2U$	$C_{48}H_{32}Cl_2F_2N_4O_4U_2$
Formula weight	1005.70	1313.73
Temperature/K	99.99(13)	100
Crystal system	orthorhombic	orthorhombic
Space group	$P2_12_12_1$	Pnna
a/Å	12.2797(2)	15.7599(16)
b/Å	12.7824(2)	17.6063(16)
c/Å	24.6681(3)	15.3755(14)
α/°	90	90
β/°	90	90
γ/°	90	90
Volume/Å^3	3872.00(10)	4266.3(7)
Z	4	4
ρ_{calc}g/cm^3	1.725	2.045
μ/mm^{-1}	4.377	3.663
F(000)	1960.0	2464.0
Crystal size/mm^3	0.201 × 0.058 × 0.025	0.13 × 0.13 × 0.12
Radiation	Mo Kα (λ = 0.71073)	synchrotron (λ = 0.7288)
2Θ range for data collection/°	3.588 to 62.054	3.606 to 54.376
Index ranges	-17 ≤ h ≤ 17, -17 ≤ k ≤ 16, -35 ≤ l ≤ 35	-19 ≤ h ≤ 19, -22 ≤ k ≤ 22, -19 ≤ l ≤ 19
Reflections collected	90543	87318
Independent reflections	10857 [R_{int} = 0.0600, R_{sigma} = 0.0402]	4407 [R_{int} = 0.0854, R_{sigma} = 0.0316]
Data/restraints/parameters	10857/0/514	4407/0/280
Goodness-of-fit on F^2	1.021	1.032
Final R indexes [I>=2σ (I)]	R_1 = 0.0246, wR_2 = 0.0430	R_1 = 0.0279, wR_2 = 0.0584
Final R indexes [all data]	R_1 = 0.0316, wR_2 = 0.0443	R_1 = 0.0394, wR_2 = 0.0625
Largest diff. peak/hole / e Å^{-3}	1.09/-0.71	1.41/-0.94
Flack parameter	-0.012(2)	

Parameter	[UO$_2$Cl$_2$(ph$_2$phen)(THF)]	Parameter	[UO$_2$Cl$_2$(ph$_2$phen)]$_2$	Parameter	[UO$_2$Cl$_2$(ph$_2$phen)$_2$]
U=O$_{yl}$ distance	1.763(2)	U=O$_{yl}$ distance	1.755(3)	U=O$_{yl}$ distance	1.777(3)
U-O$_{THF}$ distance	2.474(2)	U-Cl(bridging) distance	2.768(1)	U-Cl distance	2.688(1)
U-Cl distance	2.7023(7)	U-Cl(terminal) distance	2.644(1)	U-N distance (1)	2.615(3)
U-N distance	2.639(2)	U-N distance (1)	2.562(3)	U-N distance (2)	2.662(4)
		U-N distance (2)	2.620(3)	U-N distance (3)	2.782(3)
				U-N distance (4)	2.816(3)
O-U-O angle	177.41(8)		178.0(1)		163.4(1)

Table S 4 Key parameters (bond lengths/ Å, and angles/°) for the solid-state structures of the uranyl Ph$_2$phen chloride

5. Absorption and emission spectroscopic study of the precatalysts
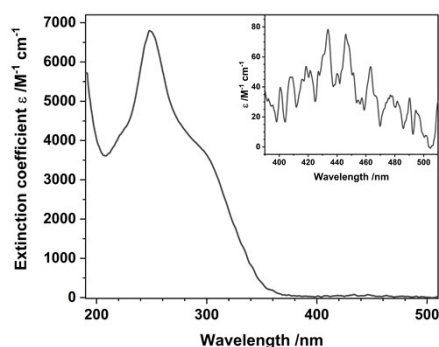
Figure S 1 Absorption spectrum of **UO$_2$Cl$_2$(THF)$_3$** in MeCN at room temperature with detail (insert).

Ph$_2$phen

Steady state absorbance and emission spectra for the **Ph$_2$phen** ligand, *Figure S 2*a, show consistent absorption and emission maxima at 273 nm and 380 nm respectively, in all solvents examined (toluene, THF, dichloromethane (DCM), MeCN). Upon excitation into the absorption bands at 300 nm, Ph$_2$phen exhibits fluorescence with a maximum at 362 nm. The excitation spectra produced when monitoring the central emission wavelength show good agreement with the absorption spectra.

Upon repetition of the measurements in frozen 2-methyl tetrahydrofuran (MeTHF) glass, *Figure S 2*b, the fluorescence emission band becomes resolved, with peaks at 356, 375, and 393 nm. Similar vibrationally resolved emission is also recorded with maxima at 476, 511, and 550 nm. The excitation spectra recorded by monitoring the emission at each of these maxima are superimposable; which indicates that the longer wavelength emission is phosphorescence.[2]

A   B
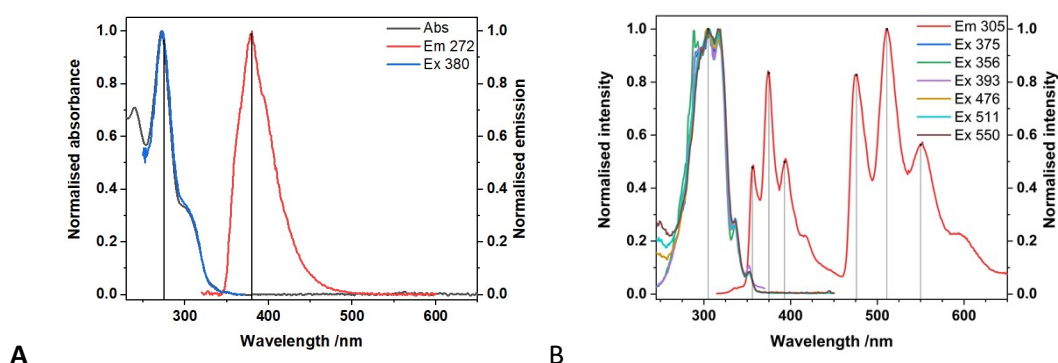
Figure S 2 Absorption (black line), emission (red), and excitation (blue) spectra of **Ph$_2$phen** in MeCN at room temperature (A) and in frozen methyl-THF at 77 K (B)

Time resolved measurements of the **Ph$_2$phen** ligand at 77 K, *Figure S 2*, support the assignment of the ca. 510 nm emission band being phosphorescence as the lifetime is substantially longer than the ca. 393 nm fluorescence band.
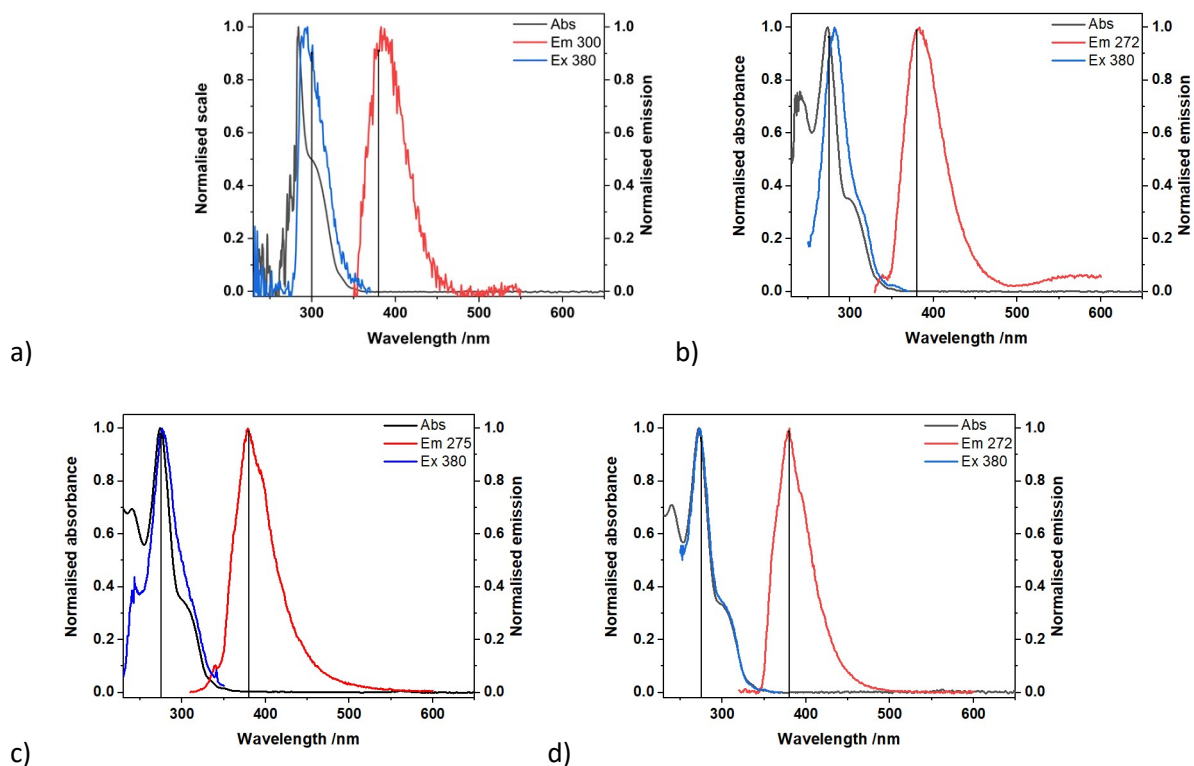
a)

b)

c)

d)

Figure S 3 Absorption (black line), emission (red), and excitation (blue) spectra of **Ph₂phen** ligand in toluene (A), THF (B), DCM (C), and MeCN (D).
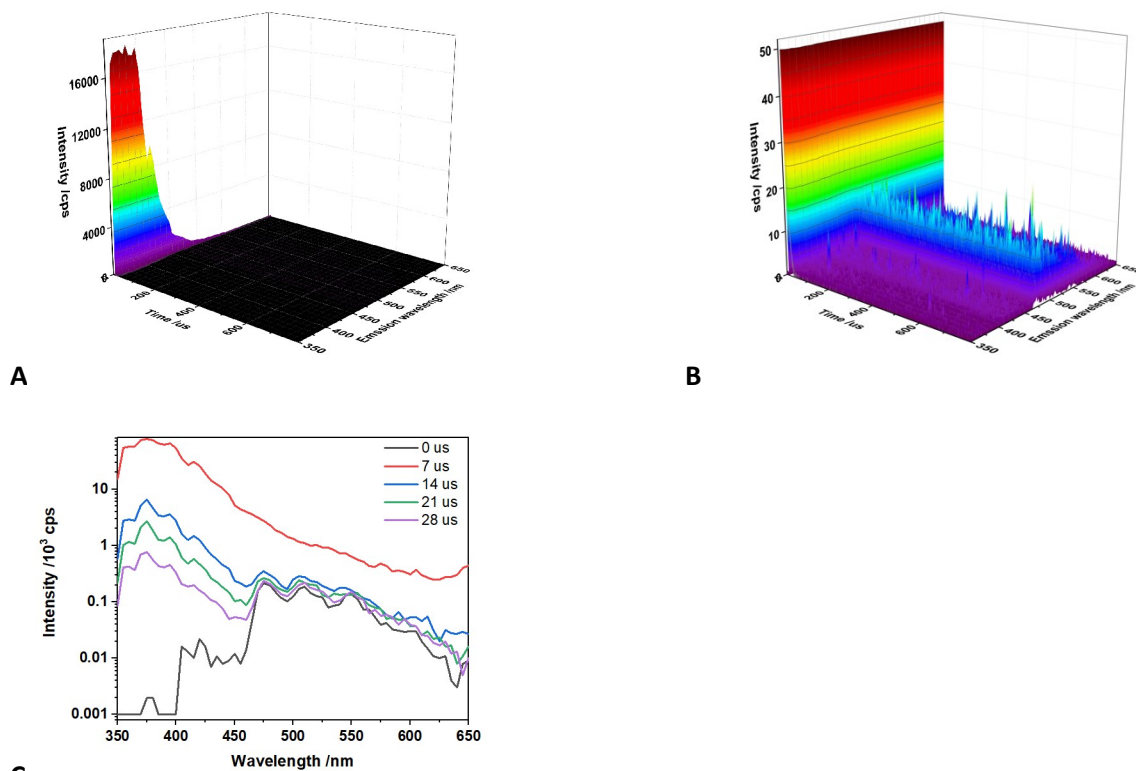

A

B

C

Figure S 4 Low temperature (77 K) time resolved emission spectra map (A, expanded B) and time sliced spectra (C) of **Ph₂phen** in frozen Me-THF showing the short lived and longer-lived emission bands are fluorescence and phosphorescence respectively.

The complexation of a single **Ph₂phen** ligand with uranyl(VI) to afford **1-NO₃** leads to a shoulder on the low energy side of the absorption envelope (350 – 400 nm), and a marked change in the solvent-dependence of the spectra, indicative of more charge transfer character, Figure S 5. The emission in THF shows residual ligand fluorescence and a broad feature centered at 573 nm, assigned to **Ph₂phen** phosphorescence whereas samples in DCM give a single emission band centred at 445 nm, which is broad and featureless, Figure S 6.

Time resolved measurements of room temperature THF solutions of **1-NO₃** Figure S 5, show that the uranyl emission is much longer lived than the equatorial LMCT emission which has decayed to near background intensity after 30 microseconds. In frozen solution at 77 K in 2-Me-THF, the uranyl emission possesses a lifetime of ~185 µs.
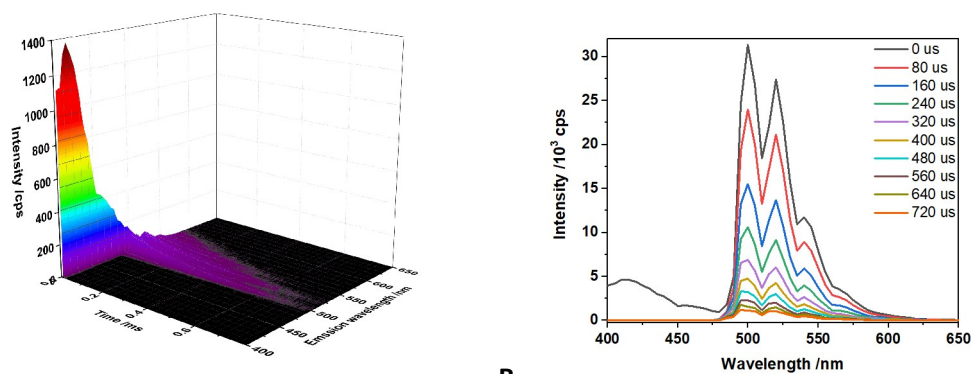
A   **B**

Figure S 5 Low temperature (77 K) time resolved emission spectra map (A) and spectra recorded with increasing time delay sliced (B) of **1-NO₃** in frozen MeTHF.

In Fig S6, B (and C), the emission max is different to the ligand (and in A, complex in THF)-suggesting that the emission in THF for complex 1 is ligand based and in DCM is uranyl based. Considering the energy of this, it is suggested that this is phen-uranium LCMT and in MeCN, phen-uranium LMCT is observed alongside the uranyl LMCT.
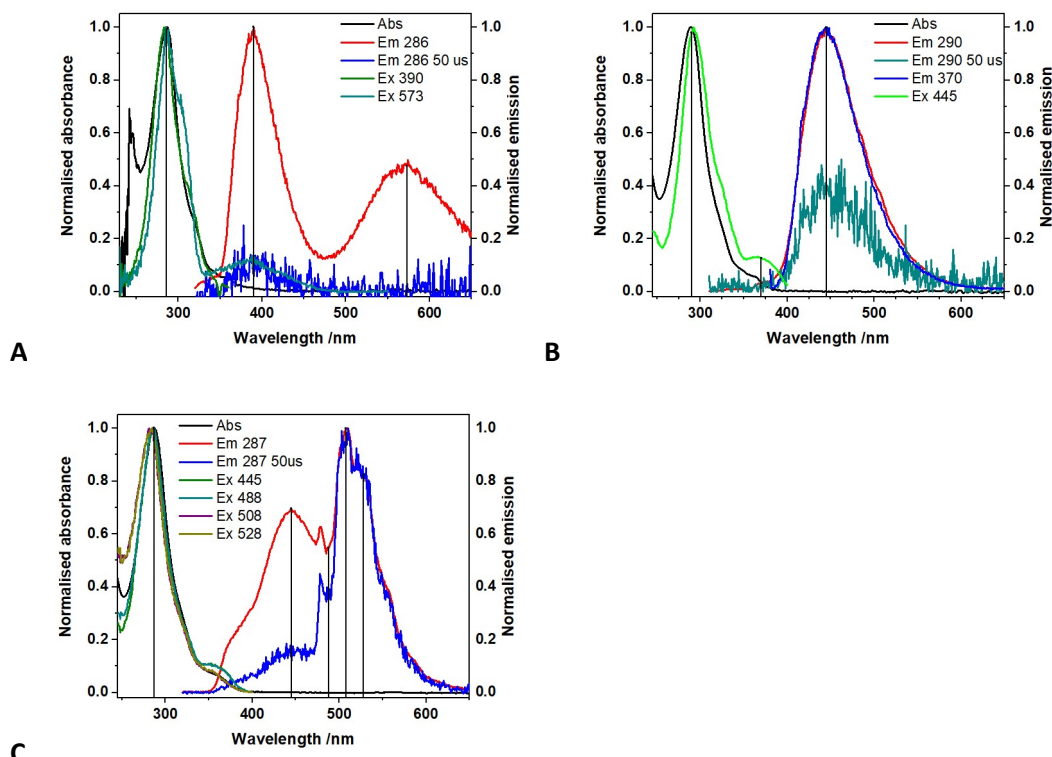
A

B

C

Figure S 6 Absorption, emission, and excitation spectra of **1-NO₃** in THF (A), DCM (B), and acetonitrile (C) at room temperature.

2 in THF or CH₂Cl₂ solution

In contrast to solutions of **2** in MeCN, solutions of **2** in THF and DCM do not release free **Ph2phen**. Thus, although not relevant to the catalysis, they are instructive for explaining the photophysics of **1-Cl.** As shown in Figure S 7, the predominant emission features are likely to be ligand-based in origin, by comparison with the emission of free **Ph2phen** in THF (λ_{em} = 390 nm) and the longer wavelength of the ligand-to-uranium charge transfer emission in DCM (λ_{em} = 445 nm).

When cooled to liquid nitrogen temperature (Figure S7) the uranyl emission of **1-Cl** exhibits better-resolved vibrational progression due to reduced non-radiative vibrational decay; this is accompanied by the disappearance of ligand fluorescence indicating that the intra ligand π-π* excitations are involved in the energy migration pathway to afford uranyl LMCT emission. These energy transfer processes are more efficient at 77 K.[3] The excitation spectrum of the uranyl(VI) emission (centered at ca. 330 nm) is also different to the absorption spectrum and exhibits vibronic fine structure (Figure S7), suggesting that, like **1-NO₃** above, the equatorial Ph₂phen-to-uranium LMCT excitation is responsible for the observed typical uranyl(VI) emission.
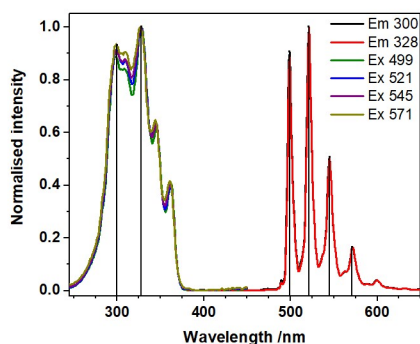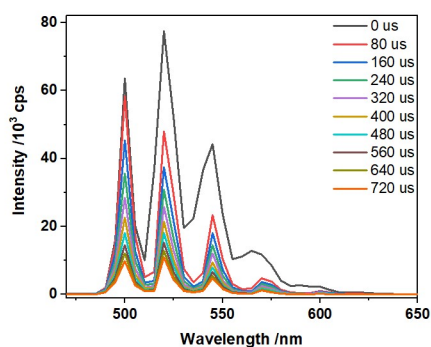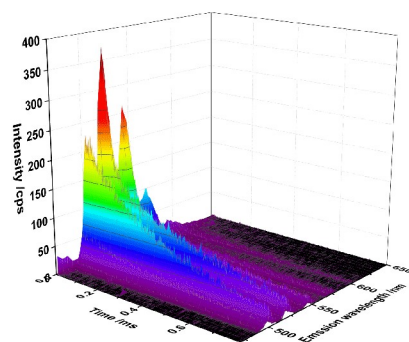
Figure S 7 Low temperature (77 K) emission and excitation spectra of **2** in frozen MeTHF.


a)   b)

Figure S 8 Low temperature (77 K) time resolved emission spectra map (A) and time sliced spectra (B) of **2** in frozen Me-THF.

Binding of the second ph$_2$phen ligand to the uranyl(VI) centre in **2** yields similar room temperature spectroscopic behavior for solutions of **2** in THF and DCM, Figure S 9, where the predominant emission features are likely to be ligand based in origin by comparison with the ligand itself in THF (λ_{em} = 390 nm) and longer wavelength ligand to uranium charge transfer emission in DCM (λ_{em} = 445 nm). However, in MeCN, (Figure S 9c), the typical uranyl(VI) LMCT emission at ca. 520 nm is clearly apparent alongside a higher energy broad feature at 381 nm, which is much shorter lived than the uranyl LMCT emission, can be removed using a time gate and is assigned to **Ph$_2$phen** fluorescence. When cooled to liquid nitrogen temperature, the uranyl emission exhibits more well resolved vibrational progression due to reduced non-radiative vibrational decay; this is accompanied by the disappearance of ligand fluorescence indicating that the intra ligand π-π* excitations are involved in the energy migration pathway to afford uranyl LMCT emission and that that these energy transfer process, are more efficient at 77 K. [3] The excitation spectrum of the uranyl(VI) emission (centered at ca. 330 nm) is also different to the absorption spectrum and exhibits vibronic fine structure, again, suggesting that the equatorial **Ph$_2$phen** to uranium LMCT excitation is responsible for the observed typical uranyl(VI) emission as observed with compound **1-NO$_3$**.
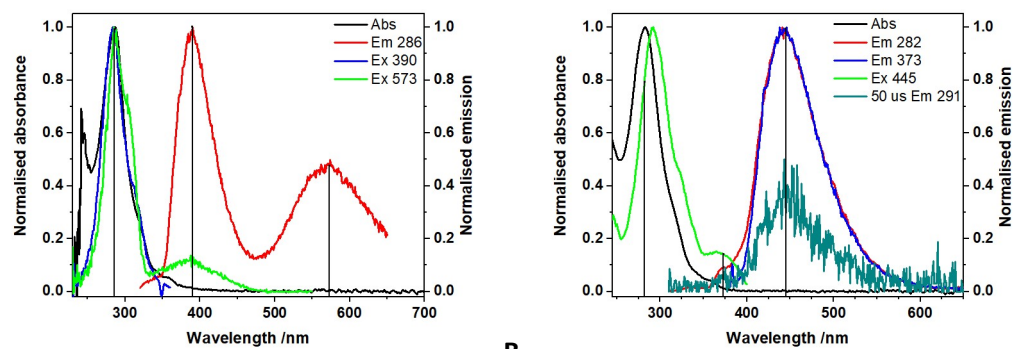
A
B

Figure S 9 Absorption, emission, and excitation spectra of **2** in THF (A) and DCM (B) recorded at room temperature in fluid solution.

The changes in uranyl complexes during the first two hours of fluorination reactions were confirmed by UVvis spectrophotometry, where the characteristic vibronic coupling is readily visible, Figure S 10. The UVvis spectra of both **1-Cl** and **U^{Cl}** reactions show small changes in the region associated with the uranyl LMCT absorption manifolds, so it is likely that these are due to some replacement of Cl by F.
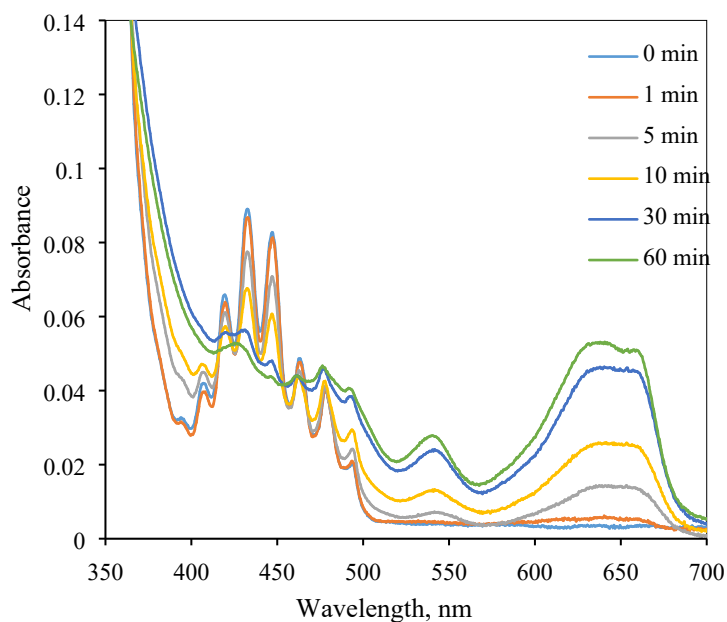
Figure S 10 Change in UVvis absorption spectra with time during the catalytic fluorination of cyclooctane by [UO$_2$Cl$_2$(MeCN)$_3$] **U^{Cl}** in MeCN.

Table S 5 Collected photophysical data for uncomplexed **Ph₂phen**, and *mono* (**1-NO₃**) and *bis* (Ph₂phen) (**2**) complexes and comparison with the uranyl(VI) precursors $UO_2(NO_3)_2$ and UO_2Cl_2 at room temperature.

		λ_{max}^{abs} /nm	λ_{max}^{em} /nm	λ_{ex} /nm	λ_{em} /nm	τ /μs (relative % contribution)	$\chi2$
Ph₂phen	Tol	284	383	375	415	4.0×10^{-4} (0.31) 3.1×10^{-3} (0.69)	1.17
	THF	273	383	*a*	*a*	*a*	---
	DCM	274	379	*a*	*a*	*a*	---
	MeCN	272	380	*a*	*a*	*a*	---
UO₂(Ph₂phen)(NO₃)₂ (1-NO₃)	THF	286	390	*a*	*a*	*a*	---
			570	*a*	*a*	*a*	---
	DCM	290	444	370	444	5.81	1.07
	MeCN	287	445	287	488	9.60	1.19
			509	287	508	10.0	1.02
			528	287	528	11.4	1.03
UO₂(NO₃)₂.6H₂O	THF	246	349	*a*	*a*	*a*	---
	MeCN	245	467	*a*	*a*	*a*	---
			486	287	485	19.4	0.98
			508	287	510	20.9	1.03
			530	287	530	18.8	1.05
UO₂Cl₂(MeCN)₃	MeCN	274	518	280	510	91.50	3.02
UO₂(Cl)₂(Ph₂phen)₂ (2)	THF	277	388	*a*	*a*	*a*	---

			571	*a*	*a*	*a*	---
	DCM	283	443	280	445	5.77	1.00
	MeCN	275	380	274	380	5.68	1.43
			479	274	480	11.0	1.02
			490	274	490	7.92 (0.54) 50.0 (0.46)	1.26
			498	274	500	8.37 (0.47) 56.9 (0.53)	1.11
			511	274	510	8.99 (0.31) 60.2 (0.69)	1.04
			519	274	520	7.23 (0.30) 67.5 (0.70)	1.04

a signal too weak to be reliably measured

Table S 6 Luminescence lifetimes for uncoordinated **Ph₂phen** ligand and complexes **1-NO₃** and **2** in MeTHF at 77 K.

	λ_{max}^{abs} /nm	λ_{max}^{em} /nm	τ_1 /ns	Rel %	τ_2 /ns	Rel %	χ2
Ph2phen	375	395	0.366	0.79	2.77	0.21	1.39
		477	0.820	0.75	4.93	0.25	1.38
		512	0.798	0.72	5.34	0.28	1.61
		550	0.690	0.86	6.42	0.14	2.87
			/µs		**/µs**		
1-NO₃	320	500	188	1.0	-	-	1.13
		520	183	1.0	-	-	1.12
		540	170	1.0	-	-	1.02
2	328	500	303	1.0	-	-	1.07
		520	27.6	0.10	399	0.90	1.03
		545	25.5	0.14	358	0.86	1.13
		570	24.3	0.24	326	0.76	1.16

Table S 7 Vibrational energy spacings for U(VI) emission from complexes **1-NO₃** and **2** (taken from spectra recorded at 77 K in MeTHF).

	λ_{max}^{em} /nm	E_{0-x}/cm^{-1} (x = 0, 1, 2)
1-NO₃	500	-
	520	769
	540	712
2	499	-
	521	846
	545	845
	571	835

6. Stern-Volmer measurements

An optically dilute solution (absorbance at the excitation emission wavelength ~0.1) of **1-Cl** and UO_2Cl_2 each compound in analytical grade MeCN was prepared. This is to negate any inner filter effects. The excitation wavelength utilised was 427 nm, which resulted in identical emission to that shown in Figure S 9c.The emission spectrum and luminescence lifetimes of the emission bands (in the absence of any quencher) and then upon increasing additions 2 μL aliquots of cyclooctane (2 - 20 μL) were recorded following indirect excitation at 427 nm and direct uranyl LMCT excitation at 427 nm and 440 nm. Spectra were recorded on an Edinburgh Instruments FLS1000 Fluorescescence Lifetime Spectrometer equipped with a 450 W steady state xenon lamp, a 5 W microsecond pulsed xenon flashlamp, with double 325 mm focal length excitation and emission monochromators in Czerny Turner configuration, and a red sensitive photomultiplier in Peltier (air cooled) housing (Hamamatsu R928P).

Data were analyzed according to the Stern-Volmer model (Eq. 1) where I is the initial UO_2^{2+} emission intensity before addition of the quencher, Q (cyclooctane), I_0 is fluorescence intensity in the presence of a quencher; K_{SV} is the Stern Volmer quenching constant Q is derived from the gradient of the slope of I_0/I *vs.* [Q] or τ_0/τ *vs.* [Q].

I/I_0 or $\tau/\tau_0 = 1 + K_{SV}[Q]$ **Equation 1**

Note that the intensity of the 444 nm emission band for **1-Cl** is essentially unaffected by increasing cyclooctane concentration and therefore its involvement in the photochemistry of **1-Cl** can be discounted. In addition, the emissive species that possesses the shorter lifetime component of the uranyl(VI) emission in **1-Cl** also shows a positive relationship with increasing substrate concentration, cyclooctane, although to a lesser extent than the longer-lived lifetime component, which is expected if dynamic quenching is significant.
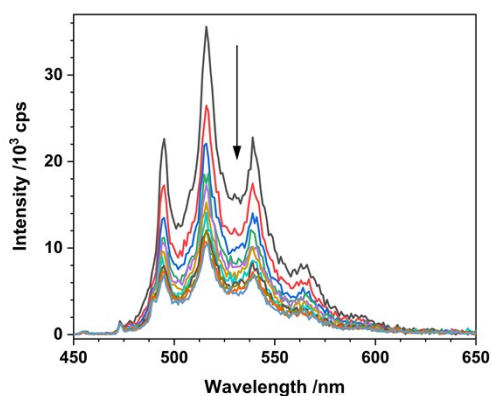
Figure S 11 Luminescence spectra samples of $UO_2Cl_2(THF)_3$ in MeCN ($UO_2Cl_2(MeCN)_3$) with increasing amounts of cyclooctane (λ_{ex} = 427 nm).
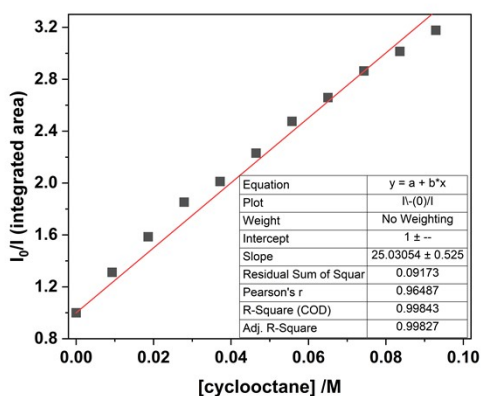
Figure S 12 Stern-Volmer plot for samples of $UO_2Cl_2(THF)_3$ in MeCN comparing the luminescence intensity with increasing amounts of cyclooctane (λ_{ex} = 427 nm).
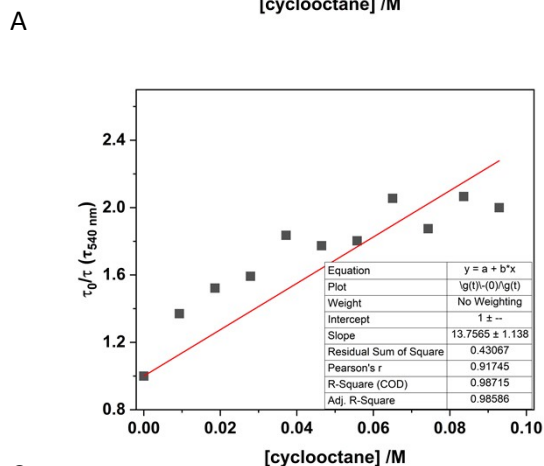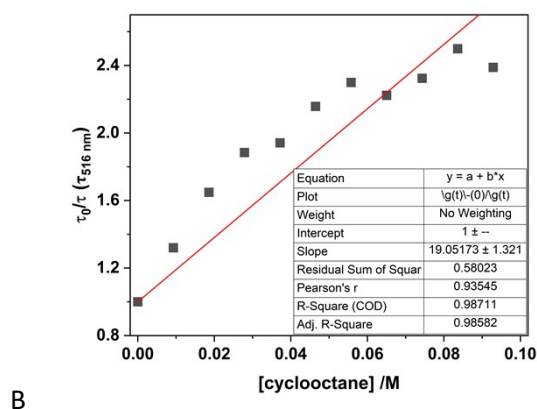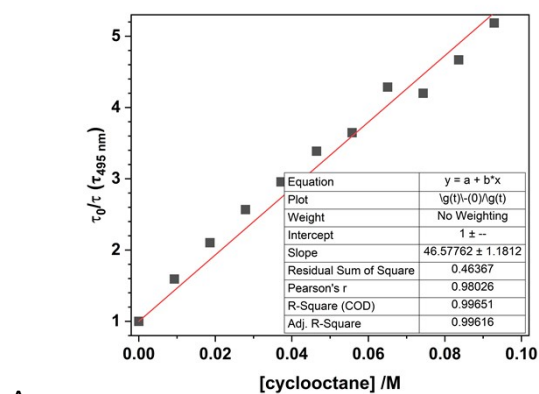

A

B

C

Figure S 13 Stern-Volmer plots for samples of $UO_2Cl_2(THF)_3$ in MeCN comparing the luminescence lifetimes at 495 (A), 516 (B), and 540 nm (C) with increasing amounts of cyclooctane (λ_{ex} = 427 nm).
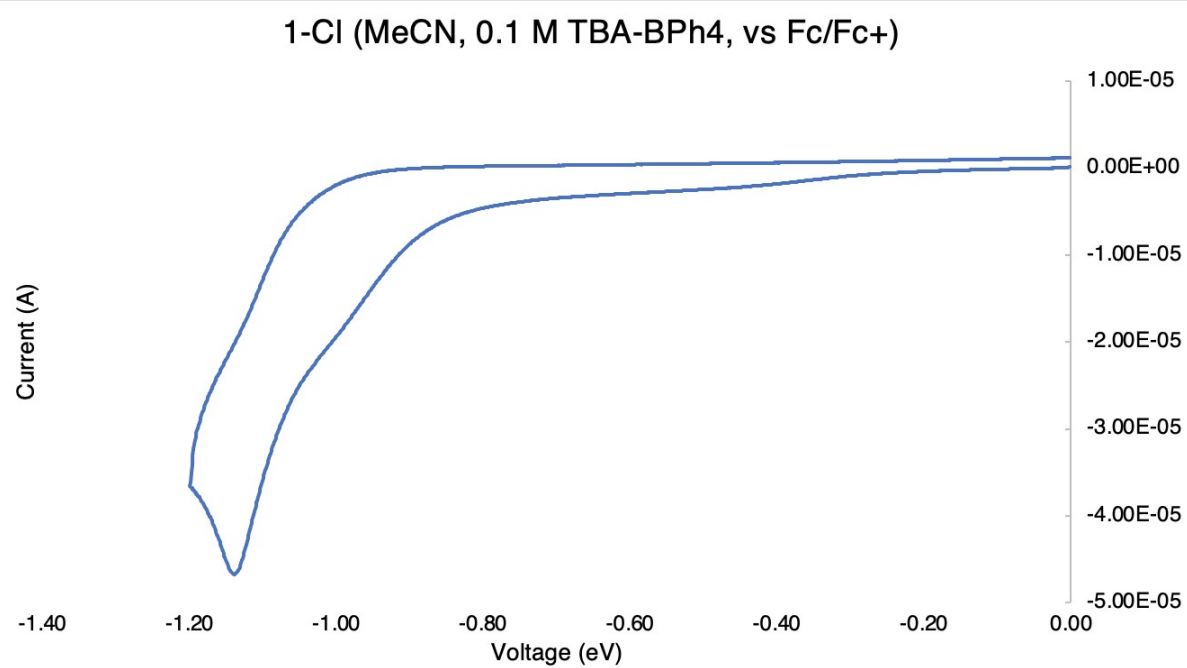
7. Electrochemistry

Figure S 14: Cyclic voltammogram for **1-Cl** in 1 mM MeCN vs Fc/Fc$^+$ (0.1 M TBA-BPh$_4$)

8. Photocatalytic activity

**General procedure for photocatalysis**

Fluorination of cyclooctane. All the reactions were performed in a nitrogen-atmosphere glovebox. A mixture of cyclooctane (81 μL, 6×10^{-4} mol, 0.6 M), NFSI (283.8 mg, 6×10^{-4} mol) and uranyl catalyst (1 mol%, 6.0×10^{-6} mol, 6.0×10^{-3} M) in acetonitrile (1 mL) was added to a 20 mL borosilicate glass vial and the solution magnetically stirred 5 cm away from a 427 nm LED lamp (Kessil PR160L 427) at ~100 rpm for 16 h. An internal standard (methyl acetate, 20 μL) was then added to an aliquot of the reaction mixture (0.4 μL) and the ^{1}H and ^{19}F NMR spectrum of the solution was recorded. The yield of fluorocyclooctane was calculated by comparing the integral of the doublet at 4.64 ppm (J = 46.4 Hz, 1H) to methyl acetate peak (3.67 – 3.45 ppm, m, 3H).

Photocatalytic oxidation. A mixture of cyclooctane (81 μL, 6×10^{-4} mol, 0.6 M) and uranyl catalyst (1 mol%, 6.0×10^{-6} mol, 6.0×10^{-3} M) in acetonitrile (1 mL) was added to a 20 mL borosilicate glass vial with a pierced lid and the solution magnetically stirred 5 cm away from a 427 nm LED lamp (Kessil PR160L 427) at ~100 rpm for 16 h. The reaction mixture was then analyzed by gas chromatography with dodecane as internal standard.

C-C coupling reactions. All the reactions were performed in a nitrogen-atmosphere glovebox. A mixture of cyclooctane (81 μL, 6×10^{-4} mol, 0.6 M), benzylidene malononitrile (92.5 mg, 6×10^{-4} mol) and uranyl catalyst (1 mol%, 6.0×10^{-6} mol, 6.0×10^{-3} M) in acetonitrile (1 mL) was added to a 20 mL borosilicate glass vial and the solution magnetically stirred 5 cm away from a 427 nm LED lamp (Kessil PR160L 427) at ~100 rpm for 16 h. An internal standard (methyl acetate, 20 μL) was then added to an aliquot of the reaction mixture (0.4 μL) and the ^{1}H and ^{19}F NMR spectrum of the solution was recorded. The yield of fluorocyclooctane was calculated by comparing the integral of the doublet at 4.58 ppm (J = 5.8 Hz, 1H) to methyl acetate peak (3.67 – 3.45 ppm, 3H).

All the organic products are known compounds and the identity of each was confirmed by comparison with the literature values.

Optimization of Fluorination reaction conditions

All the reactions were performed in a nitrogen glovebox. The mixture of substrate (6×10^{-4} mol, 0.6 M), fluorinating agent (*N*-Fluorobenzenesulfonimide, NFSI) and uranyl catalyst (1 mol%, 6.0×10^{-6} mol, 6.0×10^{-3} M) in acetonitrile was added to a 20 mL borosilicate glass vial and the solution stirred in front of a 427 nm LED lamp (Kessil PR160L 427) for 16 h. An internal standard (methyl acetate, 20 μL) was then added to an aliquot of the solution (0.4 μL) and the ^{1}H NMR spectrum of the solution was recorded. The reactions were run in duplicates unless otherwise stated.

The amount of NFSI and reaction volume were both optimized. Increasing the amount of NFSI was found to improve fluorocyclooctane yields with $[UO_2Cl_2(MeCN)]$, but have essentially no effect when a ph$_2$phen-ligated complex was used (Table S 8, entries 1-6). Even though 2 equivalents of NFSI gave the highest yield with $[UO_2Cl_2(MeCN)]$, 1.5 equiv. of NFSI was chosen for subsequent reactions as the option with better atom economy. Increasing the reaction volume was found to be detrimental to fluorocyclooctane yield with both **1-Cl-MeCN** (Table S 8, entries 7 and 8) and **2** (Table 2.1, entries 5 and 9). Lower volumes could not be tested due to the limits of catalyst solubility in acetonitrile. Trace amounts (<1% yield) of cyclooctene were observed in a number of reactions.
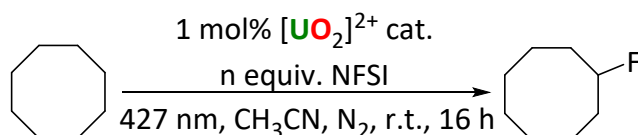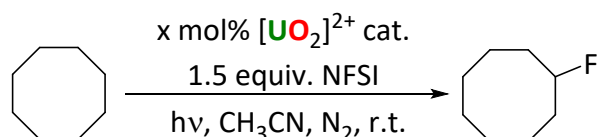

Equation S1. Photocatalytic fluorination of cyclooctane. Optimization of NFSI amount and reaction volume.

Table S 8 Cyclooctane fluorination reactions with varying NFSI loading and reaction volume.

Entry	[U] catalyst	NFSI equivalents	MeCN volume (mL)	Fluorocyclooctane yield (%)
1	[UO$_2$Cl$_2$(MeCN)]	1.0	1.0	8
2	[UO$_2$Cl$_2$(MeCN)]	1.5	1.0	26
3	[UO$_2$Cl$_2$(MeCN)]	2.0	1.0	33
4	[UO$_2$Cl$_2$(ph$_2$phen)$_2$], **2**	1.0	1.0	43
5	[UO$_2$Cl$_2$(ph$_2$phen)$_2$], **2**	1.5	1.0	40
6	[UO$_2$Cl$_2$(ph$_2$phen)$_2$], **2**	2.0	1.0	41
7	[UO$_2$Cl$_2$(ph$_2$phen)(MeCN)], **1-Cl-MeCN**	1.5	1.0	35
8	[UO$_2$Cl$_2$(ph$_2$phen)(MeCN)], **1-Cl-MeCN**	1.5	10.0	32
9	[UO$_2$Cl$_2$(ph$_2$phen)$_2$], **2**	1.5	10.0	29

Optimization of catalyst loading and concentration

Equation S2. Photocatalytic fluorination of cyclooctane. Optimization of catalyst loading and light source.

Table S 9 Cyclooctane fluorination reactions with varying catalyst loading and light source.

Entry	[U] catalyst	Catalyst loading (mol%)	LED lamp wavelength	Fluorocyclooctane yield (%)
1	[UO$_2$Cl$_2$(ph$_2$phen)$_2$], **2**	10	LED lamp (427 nm)	26
2	[UO$_2$Cl$_2$(ph$_2$phen)$_2$], **2**	1	LED lamp (427 nm)	40
3	[UO$_2$Cl$_2$(ph$_2$phen)$_2$], **2**	0.5	LED lamp (427 nm)	29
4	[UO$_2$Cl$_2$(ph$_2$phen)$_2$], **2**	1	LED lamp (440 nm)	39
5	[UO$_2$Cl$_2$(ph$_2$phen)$_2$], **2**	1	LED lamp (467 nm)	39
6	[UO$_2$Cl$_2$(ph$_2$phen)(MeCN)], **1-Cl-MeCN**	1	LED lamp (427 nm)	26
7	[UO$_2$Cl$_2$(ph$_2$phen)(MeCN)], **1-Cl-MeCN**	1	LED lamp (440 nm)	23; 4% yield of cyclooctene
8	[UO$_2$Cl$_2$(ph$_2$phen)(MeCN)], **1-Cl-MeCN**	1	LED lamp (467 nm)	25; 2% yield of cyclooctene
9	[UO$_2$Cl$_2$(ph$_2$phen)(MeCN)], **1-Cl-MeCN**	10	LED lamp (440 nm)	11; 3% yield of cyclooctene
10	none	0	LED lamp (440 nm)	trace
11	none (1 equiv. Ph$_2$phen)	-	LED lamp (440 nm)	8
12	none (2 equiv. Ph$_2$phen)	-	LED lamp (440 nm)	4
13	[UO$_2$Cl$_2$(ph$_2$phen)(MeCN)], **1-Cl-MeCN**	1	none	none
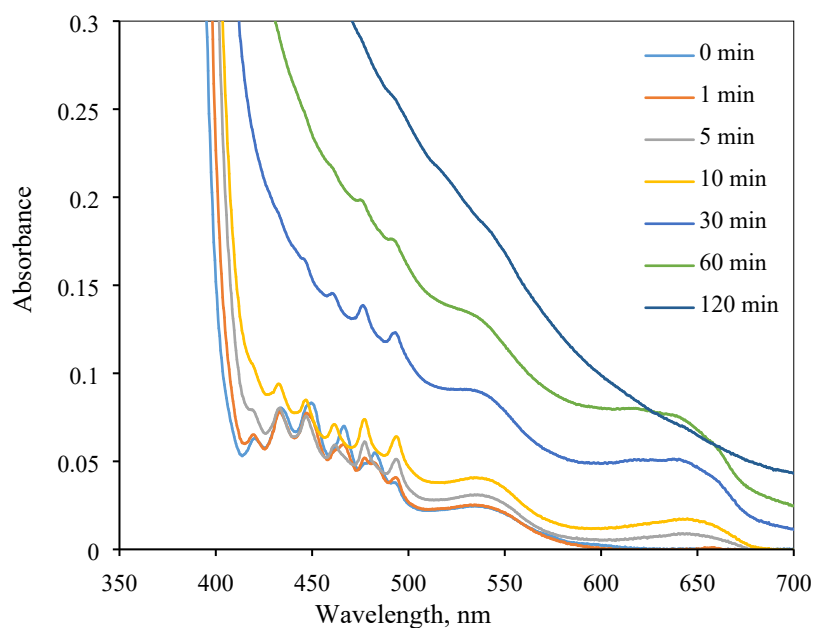
Figure S 15 Change in UVvis absorption spectra with time during the catalytic fluorination of cyclooctane by **1-Cl** in MeCN solution. The broader features arise due to a small amount of ligand decomposition which darkens the solution.
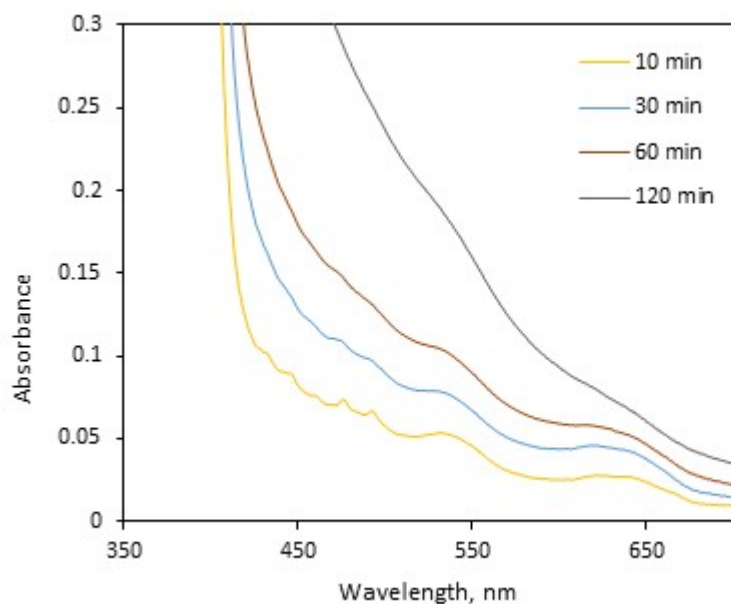

Figure S 16 Change in UVvis absorption spectra with time during the catalytic fluorination of cyclooctane by **2** in MeCN solution.

9. Computational details

Unless specified, all calculations were carried out using the ADF 2021 software package,[4, 5] the PBE[6] and PBE0[7, 8] functional with a scalar relativistic ZORA Hamiltonian,[9-11] and the small frozen core TZP basis set for all elements.[12] All geometry optimizations were carried out in conjunction with the COSMO[13] implicit solvation model. The radii values of the atomic spheres in the COSMO solvation model for atoms in this study are the corresponding van der Waals radii from the MM3 method by Allinger[14] divided by 1.2. We note that the heavy uranium metal is well buried inside of the first solvation shell and does not have direct contact with the solvation cavity. Hence, its radius setting does not affect the results of the geometry optimization. The spin-orbit coupling effect was not considered in this work as, for the types of compounds studied here, it has only a minor effect on molecular structures, vibrational frequencies, and reaction energies. Grimme's D3 dispersion[15] correction with Becke-Johnson damping (D3BJ)[16] was used for the actinyl systems. Frequency calculations were performed to ensure optimization convergence to local minima and transition states on the potential energy surface. Finally, in order to obtain higher accuracy energies in HAT reaction, single point energy correction at coupled cluster level (DLPNO-CCSD(T))[17] on the solution-optimized geometries from ADF PBE0 level were carried on using ORCA code.[18] Scalar relativistic effects were included with the ZORA Hamiltonian and the corresponding basis set ZORA-def2-TZVP.[19]

Table S 10 Selected calculated geometry parameters and Mayer Bond order for catalysts in the singlet ground state (S_0) and lowest triplet excited state (T_1) (bond lengths in Å, angles in °) at PBE/TZP/ZORA level.

[U] catalyst	parameters	S_0		T_1	
		Bond length/angle	Bond order	Bond length/angle	Bond order
[UO(NO$_3$)$_2$(H$_2$O)$_2$]	U-NO$_3$	2.502	0.37	2.544	0.34
		2.501	0.37	2.522	0.34
		2.491	0.38	2.506	0.35
		2.489	0.37	2.545	0.34
	U-H$_2$O	2.496	0.22	2.540	0.20
		2.550	0.22	2.540	0.20
	U=O	1.799	1.92	1.837	1.69
		1.799	1.92	1.836	1.69
	∠O=U=O	177.5		177.3	
[UO$_2$(ph$_2$phen)(NO$_3$)$_2$]	U-NO$_3$	2.510	0.35	2.547	0.30
		2.509	0.36	2.563	0.30
		2.507	0.34	2.545	0.29
		2.506	0.35	2.559	0.29
	U-ph2phen (eq)	2.600	0.33	2.668	0.26
		2.594	0.33	2.586	0.36
	U=O	1.804	1.91	1.834	1.84
		1.804	1.91	1.834	1.84
	∠O=U=O	177.7		177.9	
[UO$_2$Cl$_2$(MeCN)$_3$]	U-Cl	2.683	0.85	2.718	0.79
		2.684	0.85	2.720	0.79
	U-MeCN	2.565	0.30	2.581	0.29
		2.544	0.31	2.576	0.29
		2.567	0.30	2.585	0.29
	U=O	1.804	1.93	1.840	1.69
		1.804	1.93	1.840	1.69

	∠O=U=O	177.6		178.2	
	∠Cl=U=Cl	147.3		146.9	
	U-Cl	2.698	0.79	2.778	0.58
		2.696	0.80	2.778	0.58
	U-ph2phen	2.629	0.31	2.636	0.31
	(eq)	2.643	0.31	2.621	0.36
$[UO_2Cl_2(ph_2phen)(MeCN)]$	U-MeCN	2.558	0.32	2.596	0.29
	U=O	1.805	1.92	1.830	1.85
		1.805	1.92	1.831	1.85
	∠O=U=O	179.6		176.8	
	∠Cl=U=Cl	143.9		147.5	

Table S 11 Vertical excitation energies (ΔE, kcal/mol), oscillator strengths (f), and the Natural Transition Orbitals of $UO_2(NO_3)_2 \cdot 2H_2O$ calculated at the scalar–ZORA TD-DFT PBE0/TZP level of theory.
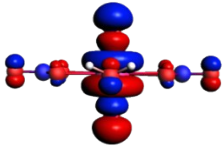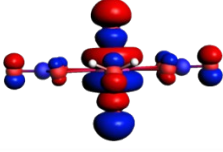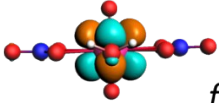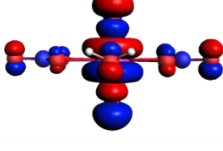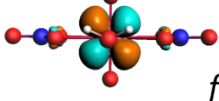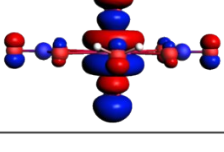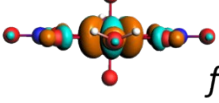
Transitions	ΔE	f	Particle	Hole
#1 $S_0 \rightarrow {}^1(\sigma_u f_{\phi1})$	86	$0.5670*10^{-5}$	σ_u	$f_{\phi1}$
#2 $S_0 \rightarrow {}^1(\sigma_u f_{\delta1})$	95	$0.1632*10^{-3}$	σ_u	$f_{\delta1}$
#3 $S_0 \rightarrow {}^1(\sigma_u f_{\delta2})$	95	$0.4524*10^{-4}$	σ_u	$f_{\delta2}$
#4 $S_0 \rightarrow {}^1(\sigma_u f_{\phi2})$	98	$0.3150*10^{-4}$	σ_u	$f_{\phi2}$

Table S 12 Vertical excitation energies (ΔE, kcal/mol), oscillator strengths (f), and the Natural Transition Orbitals of [UO$_2$Cl$_2$(ph$_2$phen)(MeCN)] calculated at the scalar−ZORA TD-DFT PBE0/TZP level of theory.
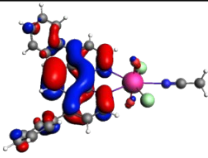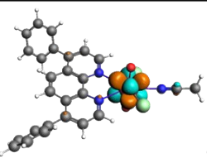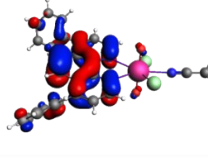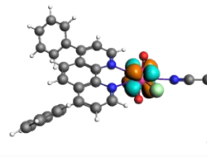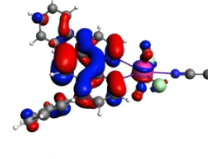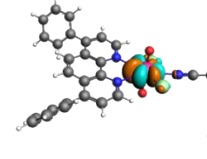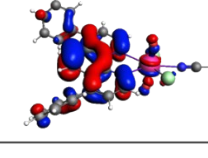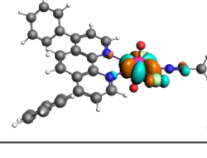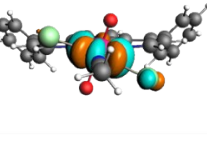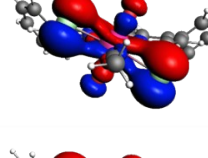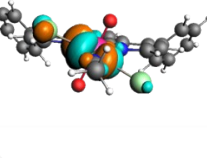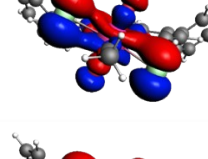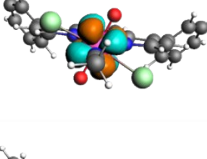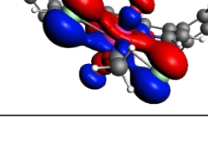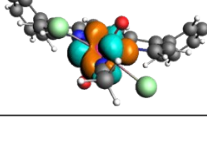
Transitions	ΔE	f	Particle	Hole
#1 S$_0$→^{1}($\pi\,f_{\phi 1}$)	74	$0.2150*10^{-1}$	π	$f_{\delta 1}$
#2 S$_0$→^{1}($\pi\,f_{\delta 1}$)	74	$0.1118*10^{-1}$	π	$f_{\delta 2}$
#3 S$_0$→^{1}($\pi\,f_{\delta 2}$)	76	$0.9503*10^{-2}$	π	$f_{\phi 1}$
#4 S$_0$→^{1}($\pi\,f_{\phi 2}$)	77	$0.2580*10^{-3}$	π	$f_{\phi 2}$

Table S 13 Vertical excitation energies (ΔE, kcal/mol), oscillator strengths (f), and the Natural Transition Orbitals of [UO$_2$Cl$_2$(ph$_2$phen)(MeCN)] calculated at the scalar−ZORA TD-DFT PBE0/TZP level of theory.

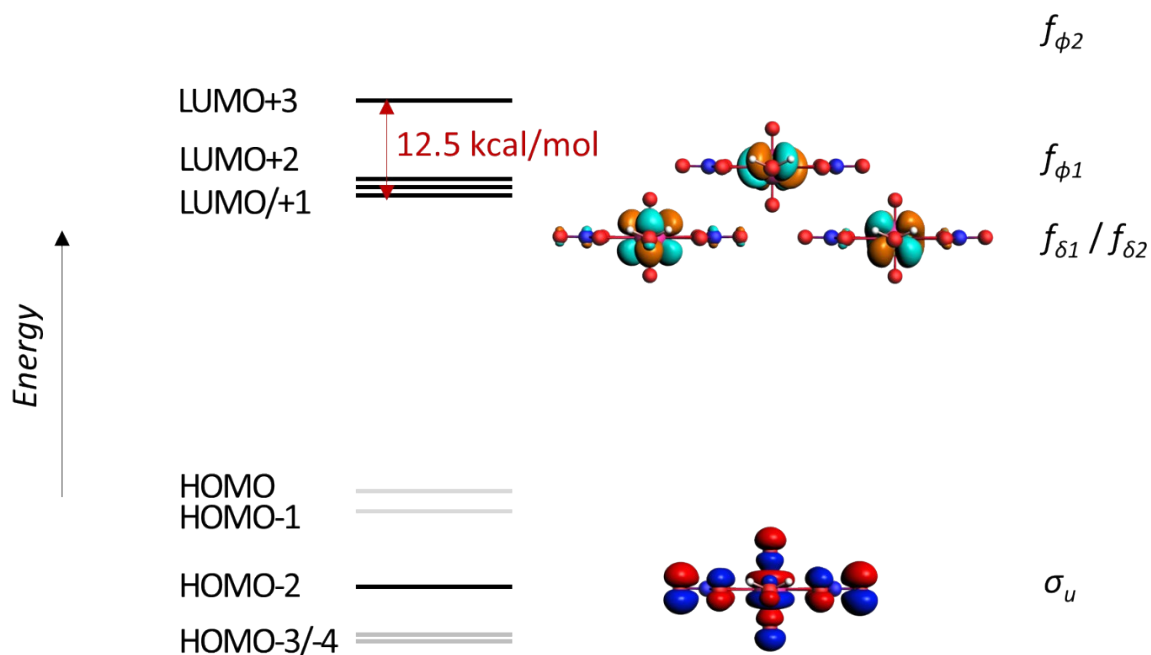| Transitions	ΔE	f	Particle	Hole
#51 S$_0$→^{1}($\sigma_u f_{\phi 1}$)	105	$0.3845*10^{-3}$	σ_u	$f_{\phi 1}$
#53 S$_0$→^{1}($\sigma_u f_{\phi 2}$)	105	$0.1233*10^{-2}$	σ_u	$f_{\phi 2}$
#54 S$_0$→^{1}($\sigma_u f_{\delta 1}$)	106	$0.3748*10^{-2}$	σ_u	$f_{\delta 1}$
#55 S$_0$→^{1}($\sigma_u f_{\delta 2}$)	107	$0.1200*10^{-2}$	σ_u	$f_{\delta 2}$

Figure S 17 The orbital energy levels for the $UO_2(NO_3)_2 \cdot 2H_2O$ catalyst calculated at the scalar–ZORA PBE0/TZP level of theory.
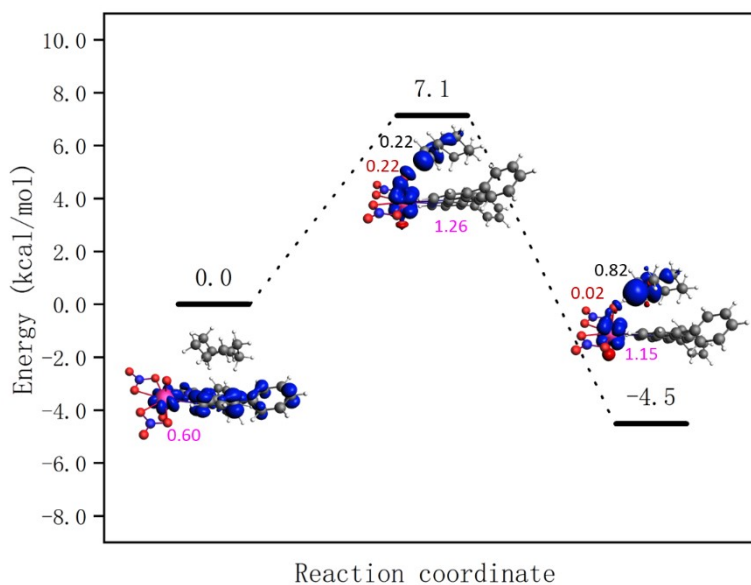

Figure S 18 Energy profiles for HAA from cyclooctane by the excited state of $[UO_2(NO_3)_2(Ph_2phen)(MeCN)]$ **1-NO₃** calculated at the DLPNO-CCSD(T)//scalar–ZORA PBE0/TZP level of theory. Spin density of reactant, transition state, and product are showed (spins on different atoms are marked in different colours: Cl – Azure, O – Red, U – Pink, and C – Black)

Table S 14 Dispersion interactions between cyclooctane and UO_2 compounds at different stages in kcal/mol calculated at the scalar−ZORA PBE0/TZP level of theory.

	S_0	T_1	TS
[$UO_2Cl_2(MeCN)_3$]	-6.9	-6.6	-6.8
[$UO_2Cl_2(ph_2phen)(MeCN)$]	-11.3	-11.9	-9.5

10. References

1.   P. L. Arnold, J. M. Purkis, R. Rutkauskaite, D. Kovacs, J. B. Love and J. Austin, *ChemCatChem*, 2019, **11**, 3786-3790.
2.   G. Accorsi, A. Listorti, K. Yoosaf and N. Armaroli, *Chem. Soc. Rev.*, 2009, **38**, 1690-1700.
3.   M. P. Redmond, S. M. Cornet, S. D. Woodall, D. Whittaker, D. Collison, M. Helliwell and L. S. Natrajan, *Dalton Trans.*, 2011, **40**, 3914-3926.
4.   G. te Velde, F. M. Bickelhaupt, E. J. Baerends, C. Fonseca Guerra, S. J. A. van Gisbergen, J. G. Snijders and T. Ziegler, *J. Comput. Chem.*, 2001, **22**, 931-967.
5.   T. Z. E.J. Baerends, A.J. Atkins, J. Autschbach, O. Baseggio, D. Bashford, A. Bérces, F.M. Bickelhaupt, C. Bo, P.M. Boerrigter, C. Cappelli, L. Cavallo, C. Daul, D.P. Chong, D.V. Chulhai, L. Deng, R.M. Dickson, J.M. Dieterich, F. Egidi, D.E. Ellis, M. van Faassen, L. Fan, T.H. Fischer, A. Förster, C. Fonseca Guerra, M. Franchini, A. Ghysels, A. Giammona, S.J.A. van Gisbergen, A. Goez, A.W. Götz, J.A. Groeneveld, O.V. Gritsenko, M. Grüning, S. Gusarov, F.E. Harris, P. van den Hoek, Z. Hu, C.R. Jacob, H. Jacobsen, L. Jensen, L. Joubert, J.W. Kaminski, G. van Kessel, C. König, F. Kootstra, A. Kovalenko, M.V. Krykunov, P. Lafiosca, E. van Lenthe, D.A. McCormack, M. Medves, A. Michalak, M. Mitoraj, S.M. Morton, J. Neugebauer, V.P. Nicu, L. Noodleman, V.P. Osinga, S. Patchkovskii, M. Pavanello, C.A. Peeples, P.H.T. Philipsen, D. Post, C.C. Pye, H. Ramanantoanina, P. Ramos, W. Ravenek, M. Reimann, J.I. Rodríguez, P. Ros, R. Rüger, P.R.T. Schipper, D. Schlüns, H. van Schoot, G. Schreckenbach, J.S. Seldenthuis, M. Seth, J.G. Snijders, M. Solà, M. Stener, M. Swart, D. Swerhone, V. Tognetti, G. te Velde, P. Vernooijs, L. Versluis, L. Visscher, O. Visser, F. Wang, T.A. Wesolowski, E.M. van Wezenbeek, G. Wiesenekker, S.K. Wolff, T.K. Woo, A.L. Yakovlev, ADF 2021.1, SCM, Theoretical Chemistry, Vrije Universiteit, Amsterdam, The Netherlands,, http://www.scm.com/).
6.   J. P. Perdew, K. Burke and M. Ernzerhof, *Phys. Rev. Lett.*, 1996, **77**, 3865-3868.
7.   J. P. Perdew, M. Ernzerhof and K. Burke, *J. Chem. Phys.*, 1996, **105**, 9982-9985.
8.   C. Adamo and V. Barone, *J. Chem. Phys.*, 1999, **110**, 6158-6170.
9.   E. v. Lenthe, E. J. Baerends and J. G. Snijders, *J. Chem. Phys.*, 1993, **99**, 4597-4610.
10. E. v. Lenthe, E. J. Baerends and J. G. Snijders, *J. Chem. Phys.*, 1994, **101**, 9783-9792.
11. E. v. Lenthe, A. Ehlers and E.-J. Baerends, *J. Chem. Phys.*, 1999, **110**, 8943-8953.
12. E. Van Lenthe and E. J. Baerends, *J. Comput. Chem.*, 2003, **24**, 1142-1156.
13. C. C. Pye and T. Ziegler, *Theor. Chem. Acc.*, 1999, **101**, 396-408.
14. N. L. Allinger, X. Zhou and J. Bergsma, *J. Mol. Struct. Theochem.*, 1994, **312**, 69-83.
15. S. Grimme, J. Antony, S. Ehrlich and H. Krieg, *J. Chem. Phys.*, 2010, **132**, 154104.
16. S. Grimme, S. Ehrlich and L. Goerigk, *J. Comput. Chem.*, 2011, **32**, 1456-1465.
17. E. Paulechka and A. Kazakov, *J. Phys. Chem. A*, 2017, **121**, 4379-4387.
18. F. Neese, *WIREs Comp. Mol. Sci.*, 2018, **8**, e1327.
19. F. Weigend and R. Ahlrichs, *Phys. Chem. Chem. Phys.*, 2005, **7**, 3297-3305.